

Investigation of Ion and Electron Conduction in the Mixed Ionic-Electronic Conductor- La-Sr-Co-Fe-Oxide (LSCF) Using Alternating Current (AC) and Direct Current (DC) Techniques

To cite this article: Chong Lei et al 2022 J. Electrochem. Soc. 169 014506

View the article online for updates and enhancements.







Investigation of Ion and Electron Conduction in the Mixed Ionic-Electronic Conductor- La-Sr-Co-Fe-Oxide (LSCF) Using Alternating Current (AC) and Direct Current (DC) Techniques

Chong Lei,* Michael F. Simpson, on Anil V. Virkar**

Department of Materials Science and Engineering, University of Utah, Salt Lake City, Utah 84112, United States of America

Among many mixed ionic electronic conductors (MIECs), lanthanum strontium cobalt iron oxide (LSCF) has been proven as a promising material for use as cathode in SOFCs. The ion and electron conduction in LSCF need to be studied separately. To measure the ionic conductivity of LSCF, YSZ disks were applied to block the electronic current, and multilayered samples were made with YSZ disks in series with an LSCF disk. Both AC and DC techniques were used for the measurements. An LSCF (porous)/LSCF(dense)/LSCF(porous) bar-shaped sample was made to measure the electronic conductivity of LSCF. DC technique was utilized for the measurement. Results show that the ionic conductivity of LSCF is much lower than its electronic conductivity. The ionic conductivity of LSCF increases with increasing temperature (600 °C–900 °C), and the electronic conductivity decreases with increasing temperature (600 °C–900 °C). Measurements were also made on a foil of silver to investigate oxygen transport through it. From this, oxygen ion conductivity through silver was estimated.

© 2022 The Electrochemical Society ("ECS"). Published on behalf of ECS by IOP Publishing Limited. [DOI: 10.1149/1945-7111/ac43d8]

Manuscript submitted September 23, 2021; revised manuscript received November 24, 2021. Published January 6, 2022. *This paper is part of the JES Focus Issue on Women in Electrochemistry*.

Sr and Fe-doped LaCoO₃, commonly described by the acronym LSCF, is a good electronic conductor and also exhibits some level of oxygen ion conductivity, depending upon the composition and temperature. As a result, it is called a mixed ionic-electronic conductor (MIEC). The typical electronic conductivity is p-type. It is generally thus considered a good candidate for an oxygen electrode in solid oxide fuel cells (SOFCs), solid oxide electrolyzer cells (SOECs), and pressure-driven oxygen separation membranes. For oxygen separation in a pressure driven system, no external voltage is applied. Transport of oxygen occurs as a coupled process of transport of O²⁻ and electrons (holes). For this reason, transport as well as electrochemical processes, are often described in terms of a surface oxygen exchange coefficient (k_{chem}) and a chemical diffusion coefficient of oxygen (D_{chem}) . The same terminology is often used in cases where the transport is electrically driven (fuel cells, electrolyzers) when LSCF is used as electrodes. The typical measurement of D_{chem} and k_{chem} is done by radio-isotope measurements^{5,6} or by conductivity relaxation.^{7–9} The latter technique involves exposing a bar-shaped sample (fully dense or porous) to an abrupt change in atmosphere with a different oxygen partial pressure. If the abrupt change in oxygen pressure involves an increase in oxygen partial pressure, oxygen is incorporated into the sample via two series steps; surface exchange (dictated by k_{chem}) and chemical diffusion (D_{chem}). Oxygen is incorporated by filling up some oxygen vacancies and releasing electron holes into the sample $(V_O^{"} + \frac{1}{2}O_2 \rightarrow O_O^x + 2h)$. This leads to a change in the conductivity (mostly electronic) as a function of time. The time dependence is typically analyzed and fit to a combined surface exchange chemical diffusion equation, from which D_{chem} and k_{chem} are obtained.^{7,9} Transport through the porous electrodes and dense membranes of LSCF (and other MIEC materials) is often described using these parameters. However, transport does not require any close association between O^{2-} and electrons/holes. Thus, the description of transport can be equally done using ionic and electronic conductivities under small applied voltages and minimal oxygen pressure difference across the membrane.

Though the electronic conductivity of LSCF is high enough, its ionic conductivity is quite low, especially when compared to YSZ. ¹⁰ Some researchers use ionic conductors such as yttria-stabilized zirconia (YSZ) or gadolinium doped ceria (GDC) to make LSCF

+ YSZ or LSCF + GDC composite materials (often by infiltration of salts solutions followed by firing) to improve the ionic conductivity of the electrodes; thus reducing the polarization resistance. However, measurement of ionic conductivity is difficult since the electronic current needs to be completely blocked. The objective of this work was to measure ionic and electronic conductivities of LSCF using DC and AC methods.

The approach reported here involves the use of dense LSCF disks (and bars) with porous surfaces layers of LSCF. For the measurement of electronic conductivity, a thin, long bar-shaped sample was used, because the electronic conductivity of LSCF under the measurement conditions is very high. These measurements were conducted by using a standard DC method. Measurement of the ionic conductivity of the MIEC is more difficult since the ionic conductivity is much lower than the electronic conductivity; the electronic current must be completely blocked. To study ion conduction in LSCF, YSZ was selected to block the electronic current since it has good oxygen ion conductivity and negligible electronic conductivity, especially at typical SOFCs operating temperatures $(\sim 800 \, ^{\circ}\text{C})$. The measurement of ionic conductivity was done using two 8YSZ disks in series for electron blocking. Measurements were made using both DC and EIS methods (over a frequency range between 1 Hz and 1 MHz). DC and EIS measurements were also made with 2 YSZ disks in series and with a silver foil sandwiched between the two YSZ disks. The objective of making DC measurements on a silver foil was to estimate the transport of oxygen through silver.

Experimental

 $LSCF(porous)/LSCF(dense)/LSCF(porous) \ disk-shaped \ sample. \\ LSCF \ ((La_{0.6}Sr_{0.4})_{0.95}Co_{0.2}Fe_{0.8}O_{3-x}) \ powder \ (Fuel Cell Materials, LSCF-HP) \ was used to make the samples. Figure 1 shows a schematic of the symmetrical LSCF(porous)/LSCF(dense)/LSCF(porous) \ disk-shaped sample. Dense LSCF disk was obtained by die-pressing, followed by sintering at 1350 °C in air for 1 h. LSCF powder was dispersed into ethanol to make LSCF ink. Porous LSCF electrodes were applied by brush-painting the LSCF ink on both surfaces of the sintered dense LSCF disk followed by firing at 1000 °C for 1 h. Gold mesh was applied on each of the porous LSCF electrodes and fired at 500 °C for 1 h.$

1) LSCF(porous)/YSZ/LSCF(porous)/LSCF(dense)/LSCF(porous)/YSZ/LSCF(porous) (YLY) multilayered sample, 2) LSCF(porous)/YSZ/LSCF(porous)/LSCF(porous)/YSZ/LSCF(porous) (YY) multilayered sample, and 3) LSCF(porous)/YSZ/LSCF(porous)/Ag/LSCF (porous)/YSZ/LSCF(porous) (YAY) multilayered sample. Notations 1) (YLY)- L for LSCF, 2) (YY)- Y for YSZ, and 3) YAY—A for Ag are

^{*}Electrochemical Society Member.

^{**}Electrochemical Society Fellow.

^zE-mail: Michael.simpson@utah.edu



Figure 1. A schematic of the LSCF(porous)/LSCF(dense)/LSCF(porous) disk-shaped sample.

used as abbreviations..—To measure the ionic conductivity of LSCF. EIS and DC tests were performed on the multilayered samples. A dense disk of LSCF was obtained by die-pressing and sintering at 1350 °C for 1h. The thickness of the dense LSCF disk was \sim 1.20 mm. YSZ disks were fabricated by pressing 8YSZ powder (Tosoh, TZ-8Y) in a die and then sintering at 1600 °C for 4 h. This high temperature was used, because the disks were not isostatically pressed. The thickness of the YSZ disk was ~1.54 mm. Both surfaces of each YSZ disk were brushpainted with a thin layer of LSCF and then fired at 1000 °C for 1 h. For LSCF(porous)/YSZ/LSCF(porous)/LSCF(dense)/LSCF(porous)/YSZ/ LSCF(porous) (YLY) multilayered sample, dense LSCF disk was sandwiched between two LSCF brush-painted YSZ disks, Fig. 2a. For LSCF(porous)/YSZ/LSCF(porous)/LSCF(porous)/YSZ/LSCF(porous) (YY) multilayered sample, only two LSCF brush-painted YSZ disks were pressed together, Fig. 2b. Also, LSCF(porous)/YSZ/LSCF(porous)/ Ag/LSCF(porous)/YSZ/LSCF(porous) (YAY) multilayered sample was prepared, a piece of silver foil (Alfa Aesar, 1.0 mm thick, 99.9%) was sandwiched between two LSCF brush-painted YSZ disks to obtain this sample (Fig. 2c). Gold mesh was applied on each end of the porous LSCF electrode of all the multilayered samples and fired at 500 °C for 1 h for EIS and DC measurements. The sample with Ag foil was made to determine oxygen transport properties through silver.

LSCF(porous)/LSCF(dense)/LSCF(porous) bar-shaped sample.—

A thin bar-shaped sample was fabricated by pressing LSCF powder in a bar-shaped die and then sintering at 1350 °C for 1 h. Porous LSCF electrodes were applied on both ends of the sintered LSCF bar by brush-painting and then firing at 1000 °C for 1 h. Three platinum strip electrodes (P1, P2, and P3) were applied along the length of the LSCF bar circumferentially at different places. The electronic conductivity was measured by using the DC method, as shown in Fig. 3. Platinum wires were attached to the three platinum strip electrodes. Gold mesh was applied on each surface of the porous LSCF electrodes and fired at 500 °C for 1 h. For DC measurements, voltage was applied across the end electrodes, and voltage between each two platinum strip electrodes was measured. Also, the current that passed through the sample was measured. The electronic conductivity was then calculated.

The morphology of the porous LSCF electrode and the dense LSCF disk was examined by using a scanning electron microscope (FEI Nova Nano SEM 630). EIS was performed by using a Solartron electrochemical interface (SI 1287) and an impedance/gain-phase analyzer (SI 1260) using a 2-probe method from 1 Hz to 1 MHz. EIS measurements were performed on the LSCF(porous)/LSCF(dense)/LSCF(porous) disk-shaped sample and the multilayered samples from 600 °C to 900 °C. DC measurements were performed on the multilayered samples and the LSCF(porous)/LSCF(dense)/LSCF(porous) bar-shaped sample. For DC measurement, DC voltage was applied by using a voltage generator (BK precision DC

regulated power supply 1621 A). Keithley 2000 meters were used for voltage and current measurements from 600 °C to 900 °C.

Results and Discussion

Figure 4a shows a cross-sectional SEM image of the dense LSCF disk sintered at 1350 °C. It is clear that a relatively dense microstructure can be obtained when LSCF is sintered at 1350 °C. Only closed porosity was observed. Figure 4b shows an SEM image of the porous LSCF electrode fired at 1000 °C. The electrode is porous with both, connected and contiguous LSCF and connected and contiguous porosity. This facilitates the transport of gaseous species through the electrode and transport of O²⁻ and electrons/holes through the contiguous LSCF.

Figure 5a shows the impedance spectra of LSCF(porous)/LSCF (dense)/LSCF(porous) disk-shaped sample over a temperature range from 600 °C to 800 °C. There is no arc above the x-axis; only a tail is observed below the x-axis in the impedance spectra. Since LSCF is a mixed ionic-electronic conductor, one would expect reduction and oxidation reactions at the two electrodes; $\frac{1}{2}O_2 + 2e' \rightarrow O^{2-}$ and $O^{2-} \rightarrow \frac{1}{2}O_2 + 2e'$ (even though the ionic conductivity of LSCF is quite low, as will be discussed later). If so, one would expect a semicircle (or a Warburg type arc; both due to gas transport as well as that related to chemical diffusion and surface exchange) above the x-axis. 13,21 The fact that none is observed may be interpreted as due to both the electrodes and the disk being of LSCF, and LSCF is a good electronic (p-type) conductor. The associated polarization is negligible. Also, increasing resistance (corresponding to low frequency, 1 Hz) with temperature represents the resistance of lead wires; as the leads are of metallic Pt. This shows that the electronic conductivity of LSCF is very high, which should be much higher than its ionic conductivity. This was confirmed by making EIS measurements without the LSCF disk and shorting the leads. The measured spectra were almost identical (Fig. 5b), consistent with the expectation that the resistance of the lead wires is much greater than that of the LSCF disk.

Figure 5a shows that the resistive component of the sample/lead wires increases with increasing frequency. This observation has been made in numerous studies, but does not appear to have been discussed in the literature. If the equivalent circuit is considered to be an inductor and a resistor in series, both primarily associated with the lead wires, one would expect a straight vertical line below the *x*-axis. The increasing resistance with frequency appears to be associated with the well-known skin effect, which shows that as the frequency is increased, the electrical current tends to be confined to a thin layer near the surface of the wire.²² The effective resistance depends on the skin depth (δ) ,²³ for wire is given by

$$\delta = \sqrt{\frac{2\rho}{\omega\mu}} \sqrt{\sqrt{1 + (\rho\omega\varepsilon)^2 + \rho\omega\varepsilon}}$$
 [1]

where ρ is the resistivity of the conductor, ω is the angular frequency of current, μ is the permeability of the conductor, and ε is the permittivity of the conductor.

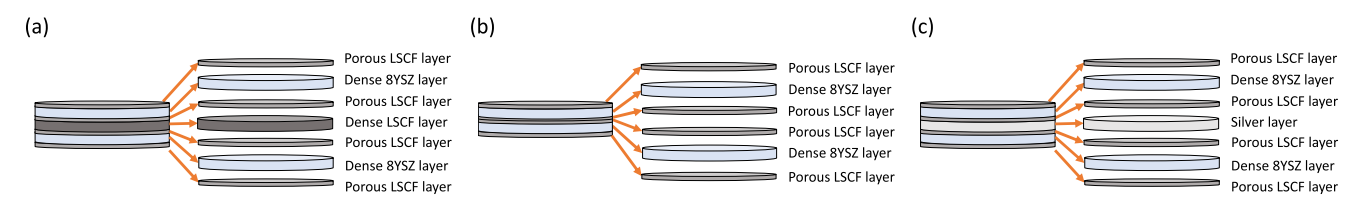


Figure 2. A schematic of (a) the LSCF(porous)/YSZ/LSCF(porous)/LSCF(dense)/LSCF(porous)/YSZ/LSCF(porous) (YLY) multilayered sample, (b) the LSCF (porous)/YSZ/LSCF(porous)/YSZ

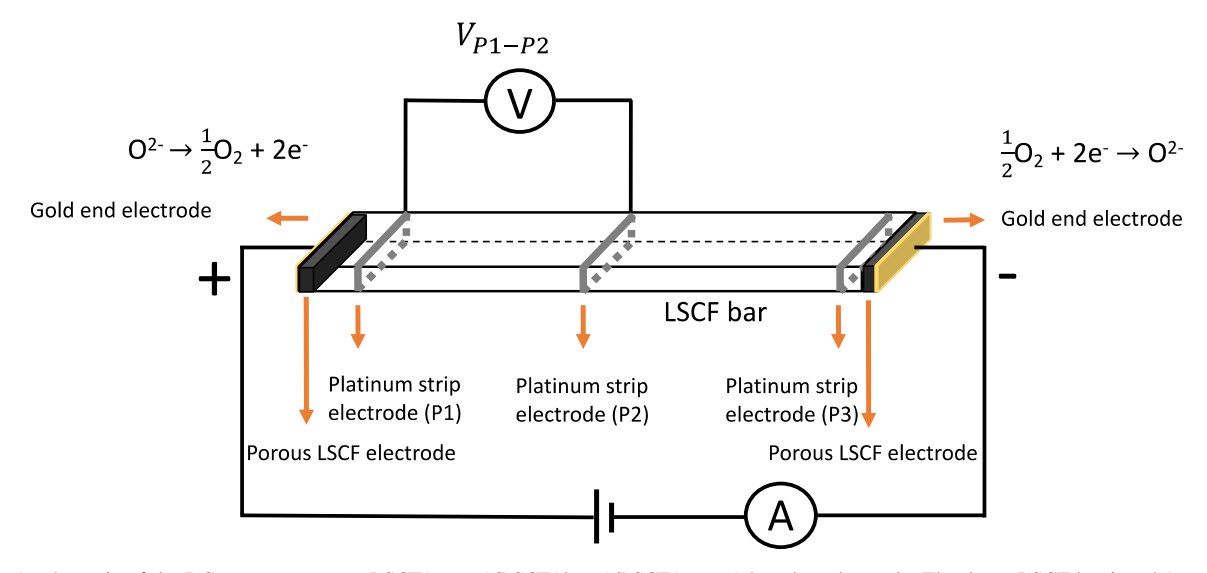


Figure 3. A schematic of the DC measurement on LSCF(porous)/LSCF(dense)/LSCF(porous) bar-shaped sample. The dense LSCF bar is \sim 4.1 cm in length, \sim 1 cm in width, and \sim 0.15 cm in thickness.

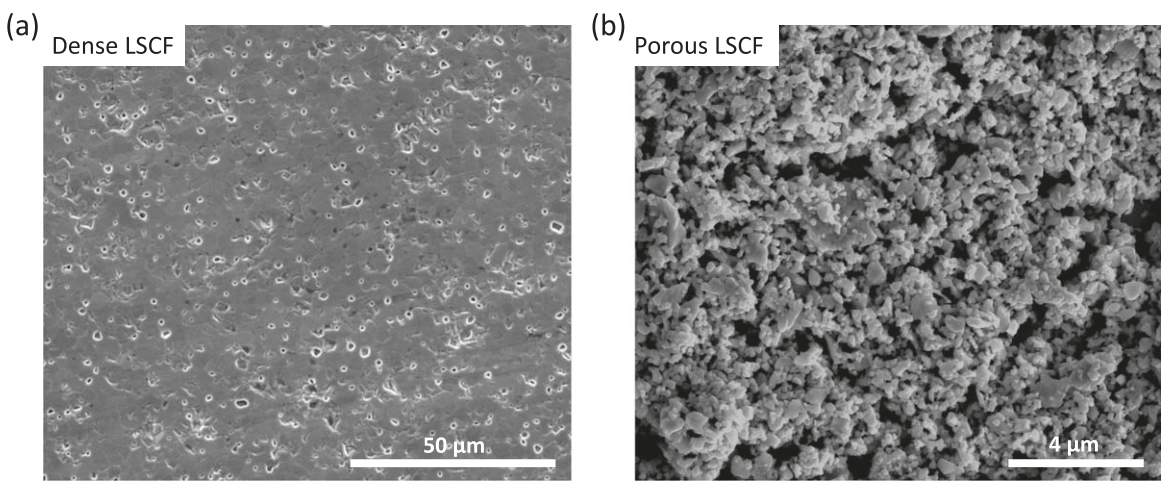


Figure 4. (a) Cross-sectional SEM image of the dense LSCF disk sintered at 1350 °C. (b) SEM image of the porous LSCF electrode sintered at 1000 °C.

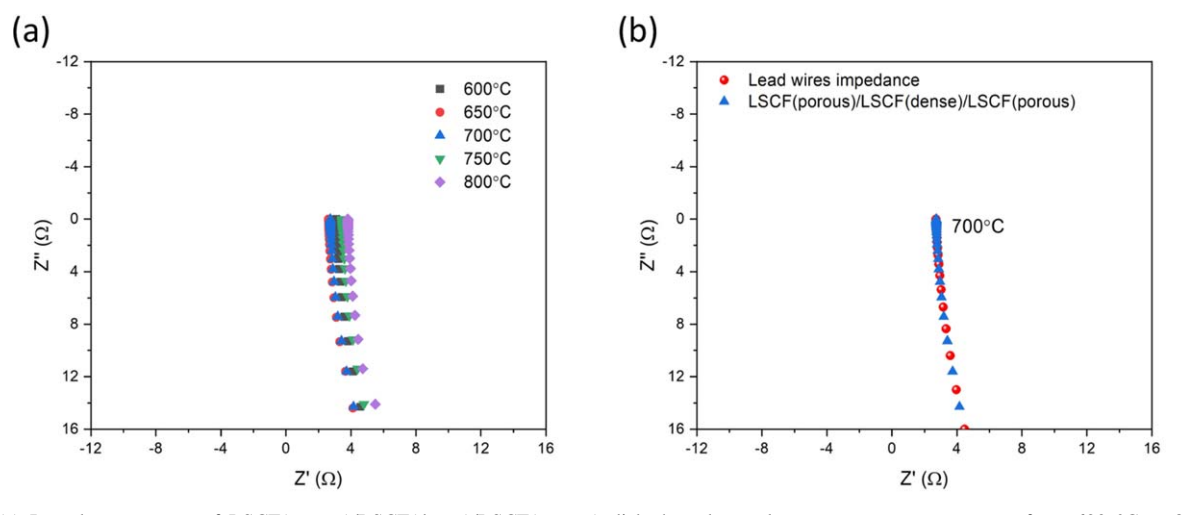


Figure 5. (a) Impedance spectra of LSCF(porous)/LSCF(dense)/LSCF(porous) disk-shaped sample over a temperature range from 600 °C to 800 °C. (b) Impedance spectra of leads resistance/inductance and LSCF(porous)/LSCF(dense)/LSCF(porous) disk-shaped sample at 700 °C.

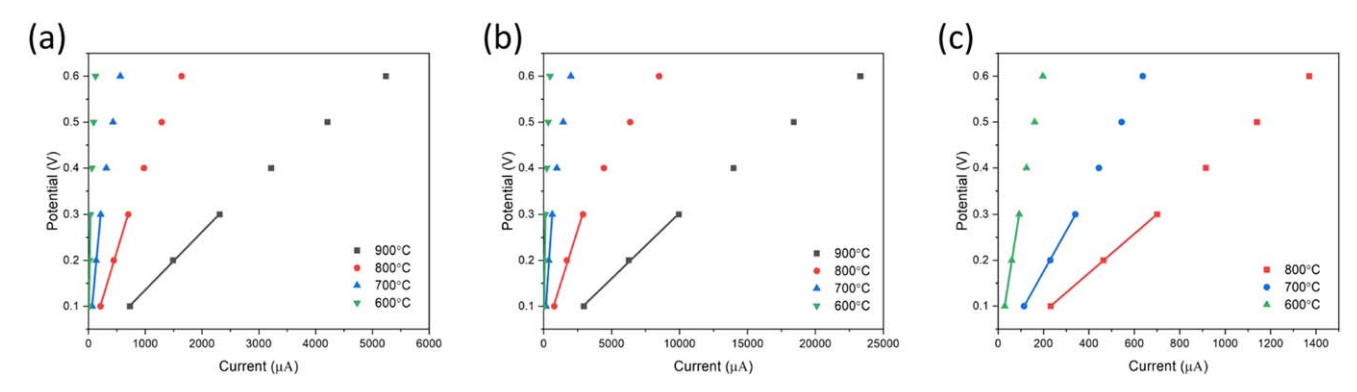


Figure 6. Potential vs current for (a) the YLY multilayered sample, (b) the YY multilayered sample, and (c) the YAY multilayered sample.

To measure the ionic conductivity of dense LSCF, DC measurements were performed on the multilayered samples. YSZ is a good oxygen ion conductor, and its electronic conductivity is negligible. Thus, YSZ disks were used to block the electronic current. Porous LSCF electrodes were applied on both surfaces of the YSZ disk to improve the contact between different layers. Figure 6 shows the applied potential vs the measured current for (a) the YLY multilayered sample, (b) the YY multilayered sample, and (c) the YAY multilayered sample. Since YSZ blocks the electronic current, only ionic current can pass through the multilayered samples. Then the ionic resistance of each multilayered sample can be calculated by using the Ohm's law. Linear fitting was used to fit all the plots at low current, and the slopes give the resistances of the multilayered samples at different temperatures. The plots are not perfectly linear at higher currents. Table I shows the resistances of the multilayered samples and the oxygen ion conductivities of dense LSCF and Ag. The ionic resistance of dense LSCF was obtained by subtracting the resistance of the YY multilayered sample from the resistance of the YLY multilayered sample. From this, the ionic conductivity of the dense LSCF can be calculated.

Subtracting DC resistance of YY multilayered sample from the DC resistance of YAY multilayered sample effectively gives the DC resistance across the Ag foil. The only transport that can occur under DC measurement is of O^{2-} . This means the following reactions occur at the YSZ/Ag and Ag/YSZ interfaces, respectively; $O^{2-} \rightarrow O + 2e'$ and $O + 2e' \rightarrow O^{2-}$. This means the transport of O^{2-} occurs as O + 2e'. Both O and O0 and O0 in metallic Ag are expected to be dissociated. Since the electronic conductivity of silver is very high, the transport of O0 is dictated by the ionic conductivity of O0 in silver; thus mainly dictated by the concentration and the diffusion coefficient of O1 in silver. The oxygen ion conductivity of silver thus is given by

$$\sigma_{O^{2-}} = \frac{2e}{k_B T} C_O D_O \tag{2}$$

where k_B is the Boltzmann constant, T is the absolute temperature, C_O is the concentration of oxygen dissolved in silver, and D_O is the oxygen diffusivity in silver.

If thus one can measure the concentration of dissolved oxygen in silver, C_O , one can in principle determine the diffusion coefficient of oxygen in silver, D_O . In principle, one can heat treat silver foils in atmospheres containing different oxygen partial pressures to change the oxygen concentration in Ag and then conduct a similar experiment as done here. This will allow one to estimate the conductivity of oxygen ions in silver as a function of oxygen concentration. This technique can also be extended to any other metal (even the ones that oxidize in air). This is because what

transports through the metal foil is O^{2-} not O. Thus, there will be no oxidation. As an example, if a sandwich structure is made with metallic Ni, and edges are sealed by some impervious glass, one should be able to measure oxygen ion conductivity through metallic nickel. Then by measuring whatever may be the oxygen concentration, one can estimate the diffusion coefficient of oxygen through it. A potentially good example is metallic Zr which can dissolve up to 29 at% oxygen in its lattice.

The oxygen ion conductivity of Ag should be very small. Table I shows the resistance of the multilayered samples and the calculated oxygen ion conductivity of dense LSCF and Ag. The measured ionic conductivity of dense LSCF is $8.48\times10^{-4}~\rm S~cm^{-1}$ at $900~\rm ^{\circ}C$, which is much lower than the reported value ($\sim\!0.18~\rm S~cm^{-1}$ at $900~\rm ^{\circ}C$) by Teraoka et al. 24 using a four-probe ionic DC technique (electron-blocking method). For their tests, not all of the electronic current was blocked by using the ionic DC technique (electron-blocking method). That may be the reason why the reported value is high. The ionic conductivity of the dense LSCF in the present work is 2.63×10^{-4} and $9.29\times10^{-5}~\rm S~cm^{-1}$ at $800~\rm and~700~^{\circ}C$, respectively, which is higher than the oxygen ion conductivity of Ag, which is $6.81\times10^{-5}~\rm and~5.07\times10^{-5}~\rm S~cm^{-1}$ at $800~\rm ^{\circ}C$ and $700~\rm ^{\circ}C$, respectively. But at a lower temperature ($600~\rm ^{\circ}C$), the dense LSCF exhibits lower ion conductivity ($1.47\times10^{-5}~\rm S~cm^{-1}$) than that of Ag ($1.88\times10^{-5}~\rm S~cm^{-1}$).

The oxygen ion conductivity of silver exhibits Arrhenius relation given by equation

$$\sigma T = \sigma_o exp \left[\frac{-E_a}{k_B T} \right]$$
 [3]

In this equation, σ is the ionic conductivity, σ_o is the pre-exponential factors, and E_a is the activation energy for oxygen ion diffusion in silver. Based on the fit shown in Fig. 7, the activation energy for oxygen ion conductivity of silver is 0.61 eV at a temperature range from 873 to 1073 K. Outlaw et al. 25 reported an activation energy for oxygen diffusion in silver, which is 0.48 eV at a temperature range from 903 to 1073 K. Our result is comparable with the reported value.

Dense LSCF exhibits low ionic conductivity, especially at low temperatures. Figure 8 shows an Arrhenius plot of LSCF ionic conductivity. The ionic conductivity of dense LSCF exhibits Arrhenius relation. The activation energy for ionic conductivity of dense LSCF is 1.26 eV. This activation energy is higher than the activation energy for ionic conductivity of common electrolytes such as YSZ and GDC. LSCF has a perovskite structure, and many perovskite oxygen ion conductors exhibit activation energy above 1 eV, depending on the composition. ^{26–28}

EIS tests were also performed on the multilayered samples. Figure 9 shows the impedance spectra of (a) the YLY multilayered sample including leads resistance/inductance, (b) the YLY

Table I. Resistances of multilayered samples and ionic conductivities of dense LSCF and Ag.									
Temperature °C	Resistance of YLY multilayered sample Ω	Resistance of YY multilayered sample Ω	Dense LSCF Ionic Resistance Ω	Dense LSCF Ionic Conductivity S/cm	Resistance of YAY multilayered sample Ω	Oxygen Ion Resistance of Ag Ω	Oxygen Ion Conductivity of Ag S/cm		
900	126.5	28.6	97.9	8.48×10^{-4}	N/A	N/A	N/A		
800	409.6	93.9	315.7	2.63×10^{-4}	427.3	333.4	6.81×10^{-5}		
700	1330	436.4	893.6	9.29×10^{-5}	884.7	448.3	5.07×10^{-5}		
600	7580	1940	5640	1.47×10^{-5}	3150	1210	1.88×10^{-5}		

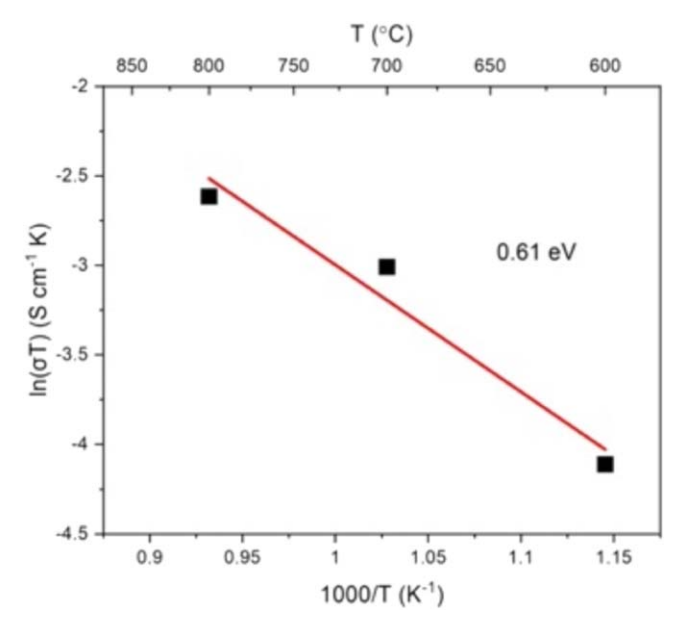


Figure 7. Arrhenius plot of the oxygen ion conductivity of Ag.

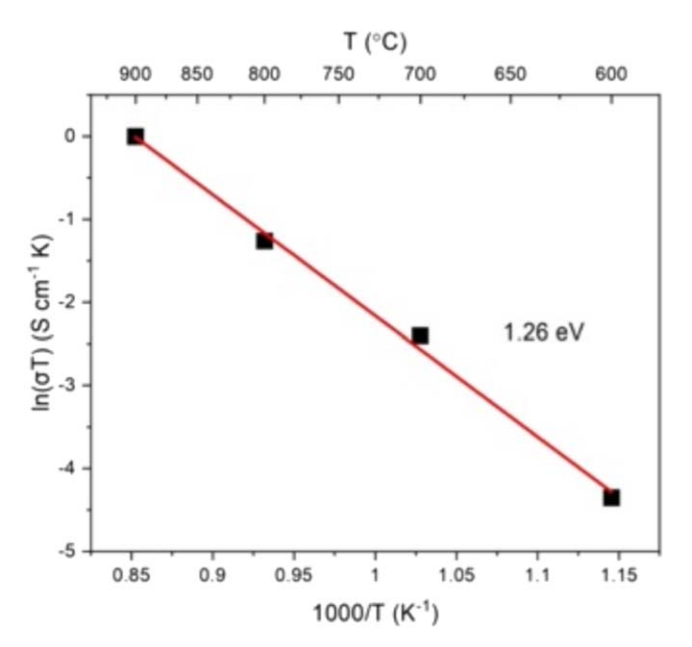


Figure 8. Arrhenius plot of LSCF ionic conductivity.

multilayered sample without leads resistance/inductance, (c) the YY multilayered sample including leads resistance/inductance, (d) the YY multilayered sample without leads resistance/inductance, (e) the YAY multilayered sample including leads resistance/inductance, and (f) the YAY multilayered sample without leads resistance/inductance. The leads resistance/inductance was subtracted point-by-point to minimize the effects from the lead wires and to obtain more accurate EIS spectra for further analysis. Table II shows the comparison of the high-frequency intercepts (after subtracting the leads resistance/inductance) of the multilayered samples, and high frequency intercepts of YLY multilayered sample and YAY multilayered sample after subtracting high frequency intercepts of YY multilayered sample from EIS spectra. The high-frequency intercept of the YY multilayered sample is very small, which is 9.7 Ω at 800 $^{\circ}$ C. The thickness of each YSZ disk is ~ 1.54 mm. This result is consistent with our previous results on LSCF(porous)/YSZ/LSCF (porous) disk-shaped sample (thickness: ~0.8 mm), which highfrequency intercept from impedance spectra is $\sim 2.3 \Omega$ at 800 °C. The thickness of the YY multilayered sample is about 4 times of the LSCF(porous)/YSZ/LSCF(porous) disk-shaped sample, and the high-frequency intercept of YY multilayered sample is also about 4 times higher than that of the LSCF(porous)/YSZ/LSCF(porous) disk-shaped sample. However, the high frequency intercept of the YLY multilayered sample and the YAY multilayered sample is much higher than that of the YY multilayered sample. This is possibly because of the skin effect. For high-frequency AC within a conductor, the current density decreases exponentially from the surface towards the inside, which reduces the effective cross-section area of the conductor and increases its effective resistance.²² The skin effect can be boosted if the permeability of the conductor is very high.³⁰ LSCF exhibits ferromagnetic behavior below 235 K, paramagnetic behavior above 235 K.³¹ The permeability of LSCF should be very high, which may contribute to the skin effect at high frequency. That is why the measured resistance of the dense LSCF or Ag by EIS is much higher than expected. Qualitatively, high resistance of dense LSCF or Ag caused by the skin effect for the multilayered sample with dense LSCF or Ag increased the measured high-frequency intercept.

Figure 10 shows the Arrhenius plots of the resistance of (a) the YLY multilayered sample after subtracting high frequency intercept of the YY multilayered sample, (b) the YAY multilayered sample after subtracting high frequency intercept of YY multilayered sample. The resistances of the dense LSCF and Ag are taken from the high-frequency intercepts from the impedance spectra after subtracting the leads resistance/inductance (Figs. 9b and 9f) and also subtracting the high frequency intercepts of the YY multilayered sample (Fig. 9d). The obtained resistances of the dense LSCF and Ag exhibits Arrhenius relation given by Eq. 4

$$\frac{R}{T} = R_o \exp\left[\frac{E}{k_B T}\right]$$
 [4]

In this equation, R is the resistance, R_o is the pre-exponential factors, and E is the activation energy in the multilayered sample. The activation energy for the dense LSCF is 0.78 eV, and the activation energy for Ag is 0.34 eV. Intuitively, one would expect that because of the good electronic conductivity of LSCF and the excellent electronic conductivity of silver, the high frequency intercepts (after the stated subtractions) should exhibit very low resistance, corresponding to predominantly electronic conduction through LSCF and Ag. But that is not the case. Once again, we believe this is related to the skin effect. At very high frequencies (1 MHz), because of the skin effect, the current remains confined to a thin region near the outer edges through both Ag and dense LSCF. This effectively leads to a very high resistance. The observed Arrhenius type behavior for Ag may be fortuitous. No thermally activated mechanism is present in silver. The possible explanation is that some effects of other components (e.g. YSZ disks) may contribute to this Arrhenius type behavior of Ag. Also, it is not possible to make a theoretical estimate. To our knowledge, there is no information available in the literature on the effect of complex experimental arrangement (e.g. 2 YSZ disks in series) would have in conduction through LSCF and Ag at high frequencies. Results are clear in DC measurements where YSZ disks serve as electron blocking electrodes, thus permitting the determination of oxygen ion conductivity through LSCF and through Ag.

For the YY multilayered sample, the total area polarization resistance of each electrode on the multilayered sample can be calculated by subtracting the high-frequency intercept from the measured DC resistance, and then dividing that number by 4 (4 layers of porous LSCF) and multiplying the surface area of the electrode. The polarization resistance of each electrode on the multilayered sample is comparable to the electrode polarization

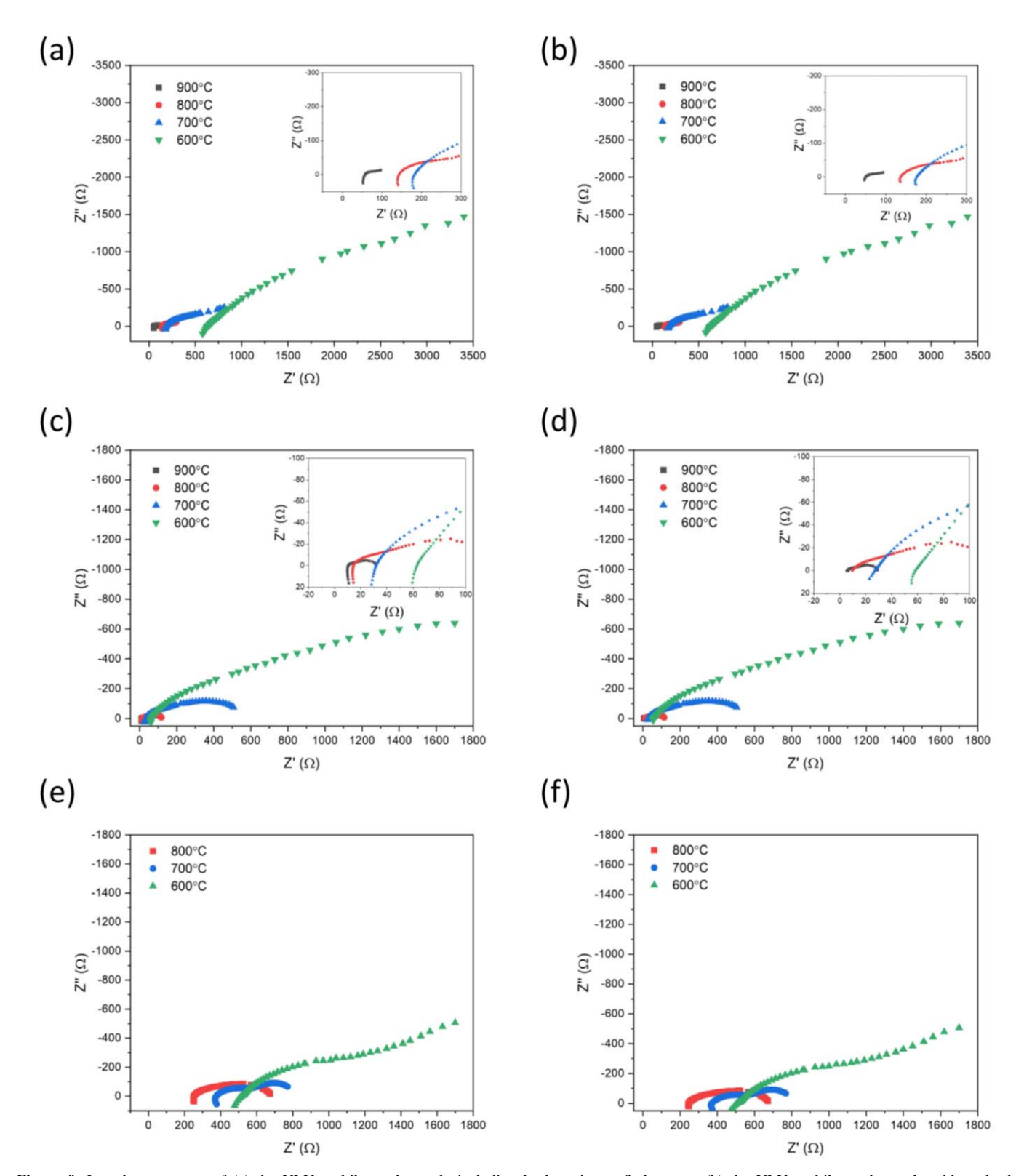


Figure 9. Impedance spectra of (a) the YLY multilayered sample including leads resistance/inductance, (b) the YLY multilayered sample without leads resistance/inductance, (c) YY multilayered sample including leads resistance/inductance, (d) the YY multilayered sample without leads resistance/inductance, (e) the YAY multilayered sample including leads resistance/inductance, and (f) the YAY multilayered sample without leads resistance/inductance.

resistance of each electrode on a symmetrical LSCF(porous)/YSZ/LSCF(porous) bar-shaped sample our group has measured by using both EIS and DC methods.²⁹ Table III shows the comparison of electrode polarization resistance on YY multilayered sample and

LSCF(porous)/YSZ/LSCF(porous) bar-shaped sample. The average total area specific electrode polarization resistance of each electrode on the multilayered sample is lower than that on the LSCF(porous)/YSZ/LSCF(porous) bar-shaped sample. We note that the examined

Table II. Comparison of high-frequency intercepts of the multilayered samples (after subtracting the leads resistance/inductance), and high frequency intercepts of the YLY multilayered sample after subtracting high frequency intercepts of the YY multilayered sample from EIS spectra.

Temperature °C	High-frequency intercept from EIS spectra Ω			Resistance calculated from high- frequency intercepts from EIS spectra Ω		
	YLY	YY	YAY	Dense LSCF	Ag	
900	50.8	6.1	N/A	44.7	N/A	
800	137.0	9.7	245.8	127.3	236.1	
700	176.3	27.0	369.8	149.3	342.8	
600	624.4	58.3	506.4	566.1	448.1	

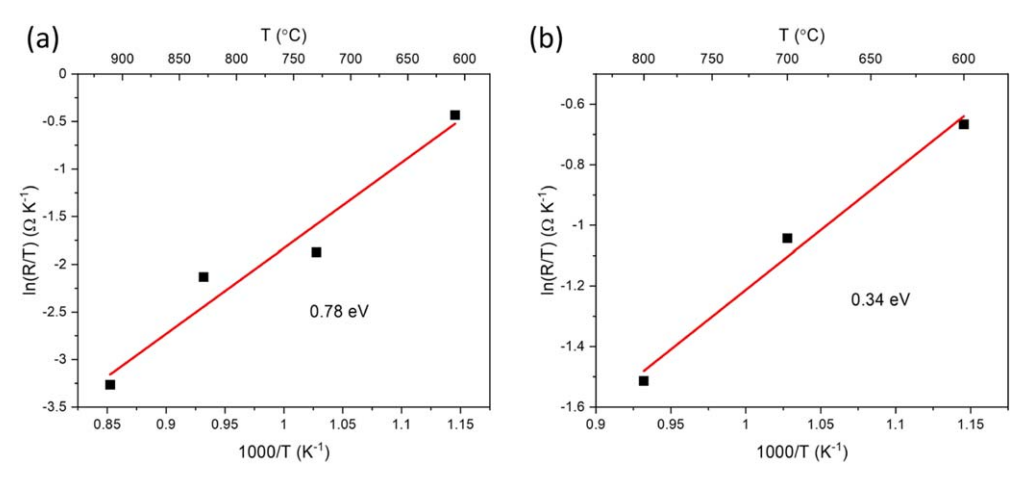


Figure 10. Arrhenius plots of the high-frequency resistance of (a) the YLY multilayered sample from which the resistance of the YY multilayered sample has been subtracted, and (b) the YAY multilayered sample from which the resistance of the YY multilayered sample has been subtracted.

current density regimes of these two samples are different. The examined current density regimes for the multilayered sample are higher than that for the LSCF(porous)/YSZ/LSCF(porous) barshaped sample. For example, at 800 °C, the average total area specific electrode polarization resistances of each electrode on the multilayered sample and the bar-shaped sample are 25.3 and 85.8 Ωcm², respectively. Nevertheless, the examined current density regimes for the multilayered sample and the bar-shaped sample are 650-2500 and 70-1400 μ A cm⁻², respectively. Since the current density for the bar-shaped sample is much lower than the exchange current density, the measured polarization resistance is much higher than the typical disk-shaped sample. However, the current density of the multilayered sample is lower than that of the bar-shaped sample but still higher than that of the typical disk-shaped sample, so the asdetermined polarization resistance is lower than the bar-shaped sample but still higher than the typical disk-shaped sample.

LSCF(porous)/LSCF(dense)/LSCF(porous) sample was made for electronic conductivity measurements. DC method was used for measuring the electronic conductivity of dense LSCF. Figure 11 shows the resistance as a function of distance, measured between the three platinum strip electrodes on the LSCF (porous)/LSCF(dense)/LSCF(porous) bar-shaped sample over a temperature range from 600 °C to 900 °C. The distance between P1 and P2 is ~ 1.76 cm, and the distance between P2 and P3 is ~1.62 cm. A certain voltage was applied across the two end electrodes. The slope gives the resistance per unit length, which is 2.72×10^{-2} , 2.43×10^{-2} , 2.14×10^{-2} , 2.12×10^{-2} Ω cm⁻¹ at 900, 800, 700, and 600 °C, respectively. The corresponding electronic conductivity of LSCF is 245.1, 274.3, 311.5, and 314.5 S cm⁻¹ at 900, 800, 700, and 600 °C, respectively. The electronic conductivity of dense LSCF is much larger than its ionic conductivity. Also, the electronic conductivity of dense LSCF increases

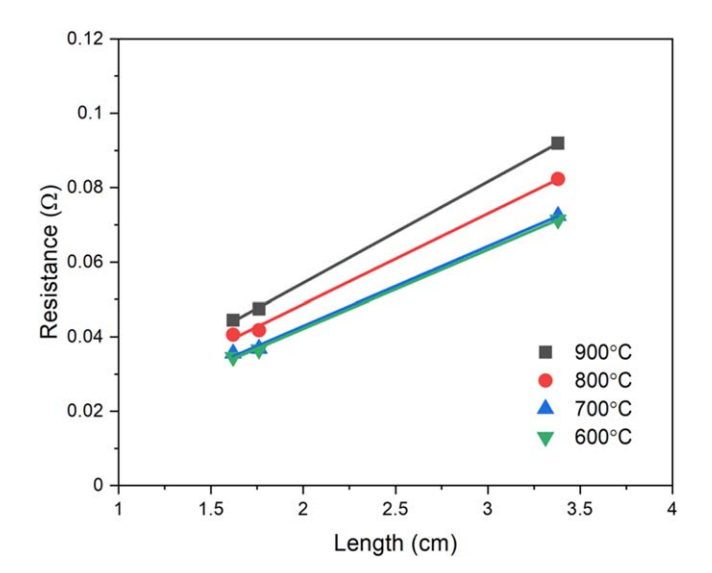


Figure 11. Resistance as a function of distance, measured between the three platinum strip electrodes on the LSCF(porous)/LSCF(dense)/LSCF(porous) bar-shaped sample over a temperature range from 600 °C to 900 °C.

with decreasing temperature. Tai et al. 32 reported that the electronic conductivity of La_{0.6}Sr_{0.4}Co_{0.2}Fe_{0.8}O₃ is $\sim\!280~S~cm^{-1}~800~^{\circ}C$. Their results also show that the electronic conductivity of LSCF reaches the maximum (at $\sim\!600~^{\circ}C$) as the temperature is increased and then it decreases as the temperature is increased. Our results are comparable to their published results.

Table III. Comparison of electrode polarization resistances on YY multilayered sample and LSCF(porous)/YSZ/LSCF(porous) bar-shaped sample.								
	YY multilayered sample		LSCF(porous)/YSZ/LSCF(porous) bar-shaped sample ²⁶					
Sample Temperature °C	Average total area specific electrode polarization resistance of each electrode Ωcm^2	Current density regime μ A/cm ²	Average total area specific electrode polarization resistance of each electrode Ωcm^2 From DC data	Current density regime μ A/cm ²				
800	25.3	650-2500	85.8	70–1400				
700	122.8	140-530	146.2	30-650				
600	564.5	28-120	1209.9	6-110				

Conclusions

The ion conduction and electron conduction in MIECs can be studied by using EIS and DC techniques. The ionic conductivity and electronic conductivity of dense LSCF were measured separately. LSCF(porous)/YSZ/LSCF(porous)/LSCF(dense)/LSCF(porous)/YSZ/LSCF(porous) and LSCF(porous)/YSZ/LSCF(porous)/LSCF (porous)/YSZ/LSCF(porous) multilayered samples were made for measuring the ionic conductivity of dense LSCF.

LSCF(porous)/YSZ/LSCF(porous)/Ag/LSCF(porous)/YSZ/LSCF (porous) multilayered sample was also made for both EIS and DC measurements. YSZ disks were used in series in these samples to block electronic current for DC measurements. The ionic conductivity of dense LSCF was measured. EIS was also performed on these multilayered samples. The high frequency intercepts of YLY and YAY were much higher than expected. This is attributed to the possible skin effect. An LSCF(porous)/LSCF(dense)/LSCF(porous) bar-shaped sample was made for measuring the electronic conductivity of dense LSCF. The electronic conductivity of dense LSCF (274.3 S cm⁻¹ at 800 °C) is much higher than its ionic conductivity (2.63 × 10⁻⁴ S cm⁻¹ at 800 °C). The present approach allows the measurement of ionic conductivity and electronic conductivity of LSCF separately.

Acknowledgments

This work was supported by the National Science Foundation under grant numbers NSF-CBET-1604008 and NSF-DMR-1742696.

ORCID

Chong Lei https://orcid.org/0000-0003-1924-290X Michael F. Simpson https://orcid.org/0000-0002-0099-0097 Anil V. Virkar https://orcid.org/0000-0003-4530-6807

References

- B. C. H. Steele and J. M. Bae, "Properties of La0.6Sr0.4Co0.2Fe0.8O3-x (LSCF) double layer cathodes on gadolinium-doped cerium oxide (CGO) electrolytes: II. Role of oxygen exchange and diffusion." Solid State Ionics, 106, 255 (1998).
- E. S. Raj, J. A. Kilner, and J. T. S. Irvine, "Oxygen diffusion and surface exchange studies on (La0.75Sr0.25)0.95Cr0.5Mn0.5O3-δ." Solid State Ionics, 177, 1747 (2006).
- J. A. Lane, S. J. Benson, D. Waller, and J. A. Kilner, "Oxygen transport in La0.6Sr0.4Co0.2Fe0.8O3-6." Solid State Ionics, 121, 201 (1999).
- A. Esquirol, J. Kilner, and N. Brandon, "Oxygen transport in La0.6Sr0.4Co0.2Fe 0.8O3-δ/Ce0.8Ge0.2O 2-x composite cathode for IT-SOFCs." *Solid State Ionics*, 175, 63 (2004).
- M. W. Den Otter, B. A. Boukamp, and H. J. M. Bouwmeester, "Theory of oxygen isotope exchange." Solid State Ionics, 139, 89 (2001).
- R. J. Chater, S. Carter, J. A. Kilner, and B. C. H. Steele, "Development of a novel SIMS technique for oxygen self-diffusion and surface exchange coefficient measurements in oxides of high diffusivity." Solid State Ionics., 53–56, 859 (1992).
- L. M. Van der Haar, M. W. Den Otter, M. Morskate, H. J. M. Bouwmeester, and H. Verweij, "Chemical diffusion and oxygen surface transfer of La1 – x Sr x CoO3 – δ studied with electrical conductivity relaxation." J. Electrochem. Soc., 149, J41 (2002).
- B. A. Boukamp, M. W. den Otter, and H. J. M. Bouwmeester, "Transport processes in mixed conducting oxides: combining time domain experiments and frequency domain analysis." *J. Solid State Electrochem.*, 8, 592 (2004).

- J. A. Lane and J. A. Kilner, "Measuring oxygen diffusion and oxygen surface exchange by conductivity relaxation." Solid State Ionics, 136–137, 997 (2000).
- B. Fan, J. Yan, and X. Yan, "The ionic conductivity, thermal expansion behavior, and chemical compatibility of La0.54Sr0.44Co0.2Fe 0.8O3-δ as SOFC cathode material." Solid State Sci., 13, 1835 (2011).
- E. Özden Çelikbilek, D. Siebert, C. L. Jauffrès, and E. D. Martin, "Influence of sintering temperature on morphology and electrochemical performance of LSCF/ GDC composite films as efficient cathode for SOFC." *Electrochim. Acta*, 246, 1248 (2017).
- Y. Leng, S. H. Chan, and Q. Liu, "Development of LSCF-GDC composite cathodes for low-temperature solid oxide fuel cells with thin film GDC electrolyte." *Int. J. Hydrogen Energy*, 33, 3808 (2008).
- J. Nielsen, T. Jacobsen, and M. Wandel, "Impedance of porous IT-SOFC LSCF: CGO composite cathodes." *Electrochim. Acta*, 56, 7963 (2011).
- J. Chen, F. Liang, L. Liu, S. Jiang, B. Chi, J. Pu, and J. Li, "Nano-structured (La, Sr) (Co, Fe)O3 + YSZ composite cathodes for intermediate temperature solid oxide fuel cells." J. Power Sources, 183, 586 (2008).
- W. G. Wang and M. Mogensen, "High-performance lanthanum-ferrite-based cathode for SOFC." Solid State Ionics, 176, 457 (2005).
- A. Pimenov, J. Ullrich, P. Lunkenheimer, A. Loidl, and C. H. Rüscher, "Ionic conductivity and relaxations in ZrO2-Y2O3 solid solutions." *Solid State Ionics*, 109, 111 (1998).
- H. Huang, M. Nakamura, P. Su, R. Fasching, Y. Saito, and F. B. Prinz, "Highperformance ultrathin solid oxide fuel cells for low-temperature operation." *J. Electrochem. Soc.*, 154, B20 (2007).
- T. Suzuki, M. Awano, P. Jasinski, V. Petrovsky, and H. U. Anderson, "Composite (La, Sr)MnO3-YSZ cathode for SOFC." Solid State Ionics, 177, 2071 (2006).
- X. Luo, Y. Yang, Y. Yang, D. Tian, X. Lu, Y. Chen, Q. Huang, and B. Lin, "Reduced-temperature redox-stable LSM as a novel symmetrical electrode material for SOFCs." *Electrochim. Acta*, 260, 121 (2018).
- T. Fukui, K. Murata, S. Ohara, H. Abe, M. Naito, and K. Nogi, "Morphology control of Ni-YSZ cermet anode for lower temperature operation of SOFCs." *J. Power Sources*, 125, 17 (2004).
- S. B. Adler, "Mechanism and kinetics of oxygen reduction on porous La1xSrxCoO3-δ electrodes." Solid State Ionics, 111, 125 (1998).
- 22. H. Wheeler, "Formulas the skin effect." Proc. IRE., 299 (1942)
- E. C. Jordan and K. G. Balmain, Electromagnetic Waves and Radiating Systems (Prentice Hall, Englewood Cliffs, New Jersey) (1968).
- Y. Teraoka, T. Nobunaga, K. Okamoto, N. Miura, and N. Yamazoe, "Influence of constituent metal cations in substituted LaCoO3 on mixed conductivity and oxygen permeability." Solid State Ionics, 48, 207 (1991).
- 25. R. A. Outlaw, S. N. Sankaran, G. B. Hoffund, and M. R. Davidson, "Oxygen transport through high-purity large-grain Ag." I Mater. Res. 3, 1378 (1988)
- transport through high-purity, large-grain Ag." J. Mater. Res., 3, 1378 (1988).
 26. H. L. Kim, S. Kim, K. H. Lee, H. L. Lee, and K. T. Lee, "Oxygen ion conduction in barium doped LaInO3 perovskite oxides." J. Power Sources, 267, 723 (2014).
- Y. Zeng, Y. S. Lin, and S. L. Swartz, "Perovskite-type ceramic membrane: Synthesis, oxygen permeation and membrane reactor performance for oxidative coupling of methane." *J. Memb. Sci.*, 150, 87 (1998).
- W. Dong, A. Yaqub, N. K. Janjua, R. Raza, M. Afzal, and B. Zhu, "All in One Multifunctional Perovskite Material for Next Generation SOFC." *Electrochim. Acta*, 193, 225 (2016).
- C. Lei, M. Simpson, and A. Virkar, "Investigation of electrode kinetics of porous La-Sr-Co-Fe-oxide (LSCF) electrodes on yttria-stabilized zirconia (YSZ) electrolyte using alternating current (AC) and direct current (DC) methods." J. Electrochem. Soc., 168, 064510 (2021).
- B. Rejaei and M. Vroubel, "Suppression of skin effect in metal/ferromagnet superlattice conductors." J. Appl. Phys., 96, 6863 (2004).
- B. Huang, J. Malzbender, and R. W. Steinbrech, "Elastic anomaly and internal friction of Ba0.5Sr 0.5Co0.8Fe0.2O3-α and La 0.58Sr0.4Co0.2Fe0.8O 3-α."
 J. Mater. Res., 26, 1388 (2011).
- L. W. Tai, M. M. Nasrallah, H. U. Anderson, D. M. Sparlin, and S. R. Sehlin, "Structure and electrical properties of La1 - xSrxCo1 - yFeyO3. Part 2. The system La1 - xSrxCo0.2Fe0.8O3." Solid State Ionics, 76, 273 (1995).